TECHNICAL ARTICLE

Fabrication and Properties of Ni$_3$Si-TiC Composites by In Situ Reaction Sintering

Muye Niu, Shuai Bao, Jianjie Wu, Xinghua Zhang, Hao Chen, and Yunxue Jin

Ni$_3$Si-based composites with different TiC contents are fabricated by in situ reaction sintering method. The phase composition, microstructure, microhardness, and tribological properties of the composites are studied. The results show that the addition of TiC particles prevents the formation of γ-Ni$_{31}$Si$_{12}$ phase, and the composites mainly consist of β_1-Ni$_3$Si and TiC phases. The composites have high hardness and relative density, and the values are above 580 HV and 87%, respectively. The friction coefficients are as low as 0.22. The wear rates of the composites are in the order of 10^{-6} mm^3 m^{-1}, which are two orders of magnitude lower than that of Ni$_3$Si alloy. The primary wear mechanism of Ni$_3$Si alloy is oxidation wear and slight abrasive wear, and the composites with TiC addition are oxidation wear and fatigue wear. The incorporation of TiC particles improves the tribological performance of Ni$_3$Si alloy significantly. The composite with 20 wt.% TiC has the optimal tribological property.

1. Introduction

Intermetallic alloys have attractive properties including good high-temperature strength, relatively low density, excellent high-temperature oxidation, and corrosion resistance and therefore exhibit a great potential application in harsh environments. The major obstacles to using the alloys are their low ductility at ambient temperature while alloying and microstructural control can significantly improve the ambient-temperature ductility (Ref 1, 2). For these reasons, intermetallic matrix composites (IMCs) are considered to be applied in aeroengine and automotive components, nuclear and power generation equipment, and extreme environments. For example, titanium aluminides-based composites have wide application prospects in the engine component, such as compressor, turbine, and combustor (Ref 3). The relevant studies also show that IMCs have excellent wear, high-temperature oxidation resistance, and corrosion resistance (Ref 4-7). Meanwhile, metallic silicides present better properties than metallic aluminides, and thus Ni$_3$Si-based composites can be regarded as potential high-performance structural materials.

The typical preparation methods of Ni$_3$Si materials are arc melting (Ref 8-10), laser cladding (Ref 11-13), and self-propagating high-temperature synthesis (Ref 14-16). But both high preparation temperature and fast cooling rate lead to the formation of by-products and aggregation of the reinforcements, which occur easily in the composites during the smelting process. Although the preparation temperature of self-propagating high-temperature synthesis is very low, the composition system is very limited. Reaction sintering is a method that can solve these problems effectively during the preparation of the composites. In the meantime, some studies have shown that reaction sintering can be used for the preparation of Ni$_3$Si-based alloys. Van Dyck et al. produced Ni$_3$Si-based alloys by reactive powder metallurgy combined with hot isostatic pressing and considered the reaction mechanism and densification process of Ni$_3$Si alloys (Ref 17). Miura et al. prepared Ni$_3$(Si,Ti) intermetallic alloy by the spark plasma sintering (SPS) method using elemental powders (Ref 18). The results showed that the sintered alloy had a high relative density in the range of 96-99%, and the high-temperature hardness and yield stress of the sintered alloys were higher than those of the cast alloys. Niu et al. fabricated Ni$_3$Si alloy from elemental powders by vacuum hot-press sintering method and studied the tribological properties under different conditions (Ref 19-22). These results demonstrated that the alloy possessed lower friction coefficient and wear rate in low vacuum condition as compared to high vacuum and air conditions; the tribological properties of Ni$_3$Si alloys with Ti addition are better than that of Ti6Al4V alloy under seawater condition; Ni$_3$Si alloy with Ti addition showed better wear resistance at high temperatures as compared to pure Ni$_3$Si alloy, and the wear rates were in the magnitude of 10^{-5} mm^3/N m. So, it is possible to prepare Ni$_3$Si-based composites, and the microstructure and properties of the composites should be investigated.

It is well noted that TiC possesses many desirable properties, such as high hardness, low density, high modulus, and high corrosion and wear resistance. Hence, TiC is a suitable candidate for being used as a reinforcement in composites. In addition, the wettability between TiC and Ni is relatively good. In this study, TiC-reinforced Ni$_3$Si-based composites

Muye Niu and **Yunxue Jin**, School of Materials Science and Engineering, Jiangsu University of Science and Technology, Zhenjiang 212003, China; and National Demonstration Center for Experimental Materials Science and Engineering Education, Jiangsu University of Science and Technology, Zhenjiang 212003, China; and **Shuai Bao, Jianjie Wu, Xinghua Zhang,** and **Hao Chen**, School of Materials Science and Engineering, Jiangsu University of Science and Technology, Zhenjiang 212003, China. Contact e-mails: nmy3015@126.com and zhangxinghua419@163.com.

were fabricated by in situ reaction sintering, which had not been reported so far. The formation mechanism of Ni_3Si-based composite was discussed, and the influence of TiC content on microstructures and mechanical properties of Ni_3Si-TiC composites was also studied. The tribological properties of the composites were investigated in detail. The effects of load and TiC content on the wear behaviors were discussed. This research provided a theoretical foundation for the application of the composites in harsh environments.

2. Materials and Methods

Ni_3Si-based composites were prepared by vacuum hot-pressed sintering method. The raw materials were commercial powders of nickel (99.8% purity, 325 mesh), silicon (99.5% purity, 300 mesh), titanium (99.5% purity, 325 mesh), boron (98.5% purity, 200-300 mesh), and TiC (99.95% purity, about 80 nm) (in mass percent). The compositions of the composites are listed in Table 1. The addition of Ti is positive to improve the toughness of Ni_3Si alloy. The samples doping with 50 wt. ppm boron is effective to suppress the intergranular fracture due to environmental embrittlement at room temperature (Ref 23). These powders were mixed evenly for 8 h in a planetary ball-mill machine (Pulverisette 6, Germany). The mixed powders were placed in graphite molds and were then pressed into cylindrical compacts with dimensions of ϕ 50 mm × 10 mm using a vacuum hot-press machine (VHP200/20-2000, China). The sintering conditions were in the temperature range of 1100 °C-1200 °C and at a pressure of 30 MPa for 40 min. The sintered samples were homogenized at 800 °C for 4 h.

The phase compositions were identified using a Shimadzu XRD 6000 diffractometer (Japan) equipped with Cu-K$_\alpha$ radiation at 40 kV and 30 mA. The 2θ scan range was from 20 to 80° with a step size of 5°/min. The microstructures and surface morphologies of the composites were studied using a scanning electron microscope (SEM, JEOL JSM-6480, Japan) equipped with an energy-dispersive spectrometer (EDS, Oxford INCA X-Act, UK). The samples were etched for 15 s in the solution of HF and H_2O_2 before the microstructural analysis. The densities of the composites were calculated by Archimedes' principle using deionized water as the immersion medium at room temperature. The relative densities were calculated using the relation:

$$D = \left(\frac{d_m}{d_{th}}\right) \times 100\% \qquad (Eq\ 1)$$

where D is the relative density, d_m is the measured densities, and d_{th} is the theoretical density. The theoretical densities are calculated from the XRD measured lattice parameters. The

microhardnesses of the samples were measured using a semiautomatic microhardness tester (HXS-1000 TAC, China) at a load of 0.5 kg and a dwell time of 10 s. The tribological tests were carried out by a ball-on-disk tribometer (HT-1000, China). The test samples were machined to the size of 20 mm diameter and 3 mm thickness. The counterpart ball was the commercial Si_3N_4 ceramic ball with a diameter of 5 mm (hardness 15 GPa). The applied load was in the range of $5 \sim 20$ N, the sliding speed was 0.10 m/s, and the sliding time was 30 min. The volumetric wear rate was calculated using the equation:

$$W = \frac{AL}{S} \qquad (Eq\ 2)$$

where W is the wear rate ($mm^3\ m^{-1}$), A is the cross-section area of the worn track (mm^2), L is the perimeter of the circular track (mm), and S is the total sliding distance (m). The cross sections of the worn tracks were measured using a laser confocal microscope (Olympus, LEXT-OLS4000, Japan). The chemical states of Ni, Si, Ti, and C elements on the worn surface of the composites were examined by an X-ray photoelectron spectroscope (XPS, Thermo Scientific Nexsa, USA). The XPS utilized monochromatic Al-K$_\alpha$ radiation at 1486.6 eV.

3. Results

3.1 Microstructure and Mechanical Properties of the Composites

The XRD patterns of the composites with different TiC content are presented in Fig. 1. It can be seen that the sample without TiC addition is composed of β_1-Ni_3Si and a small amount of γ-$Ni_{31}Si_{12}$ phase. With the addition of TiC particles, the main phase compositions of the composites are β_1-Ni_3Si and TiC phase. It should be noted that the peak intensities of γ-$Ni_{31}Si_{12}$ phase of the composites decrease significantly compared to Ni_3Si alloy, and the intensities are similar in all the composites. According to the phase diagram of the Ni-Si system, the liquid phase can appear at the temperature exceeding 1143 °C. The higher sintering temperature and liquid phase are conducive to the reactions among the elements;
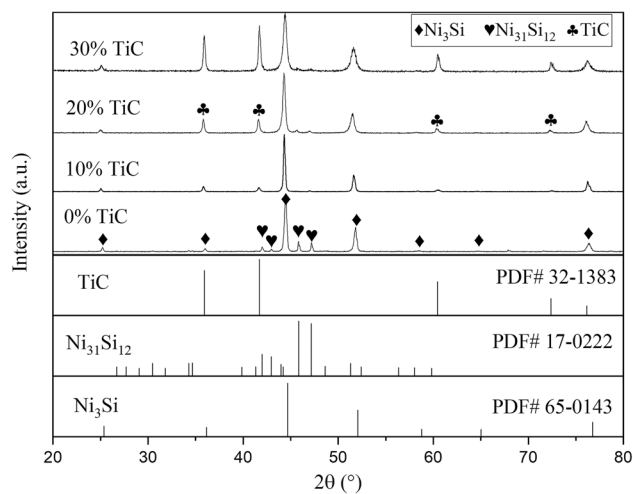
Table 1 Compositions and sintering temperatures of the composites used in this study

No	Composition	Sintering temperature
1	$Ni_{75}Si_{20}Ti_5$ + 0 wt.% TiC	1100 °C
2	$Ni_{75}Si_{20}Ti_5$ + 10 wt.% TiC	1140 °C
3	$Ni_{75}Si_{20}Ti_5$ + 20 wt.% TiC	1170 °C
4	$Ni_{75}Si_{20}Ti_5$ + 30 wt.% TiC	1180 °C

Fig. 1 XRD patterns of Ni_3Si-TiC composites

especially, the element of Ti can cause γ-$Ni_{31}Si_{12}$ phase to transform into Ni_3Si phase (Ref 19). In addition, TiC particles play a role of isolation, which separates the metallic powders in a small area. As the reaction between nickel and silicon occurs, the formed $Ni_{31}Si_{12}$ phase can further react with the nearby nickel and titanium elements to form the Ni_3Si phase. Therefore, there is almost no γ-$Ni_{31}Si_{12}$ phase in the composites with the addition of TiC. Compared to the standard spectrum of Ni_3Si, the diffraction peaks of Ni_3Si phase shift to lower angles in all the samples. It is worth noting that x-ray diffraction cannot distinguish between α-Ni and β_1-Ni_3Si, because both phases have similar structures and lattice parameters.

The microstructures of Ni_3Si-TiC composites are shown in Fig. 2. It is clear that no apparent defect is observed in Ni_3Si alloy, and the microstructure of the alloy is relatively compact, as shown in Fig. 2(a). The microstructure of the alloy consists of two regions: The dark phase is the silicon-rich region, and the composition is 68.51Ni-31.49Si (at.%); the bright phase is the nickel-rich region, and the composition is 81.41Ni-14.69Si-3.90Ti (at.%). Combined with XRD analysis, the dark region is the γ-$Ni_{31}Si_{12}$ phase which contains almost no titanium. The bright region is a eutectic structure, and the compositions are 76.97Ni-19.03Si-4.00Ti and 86.55Ni-10.98Si-2.47Ti, respectively. According to the ternary phase diagram of Ni, Si, and Ti (Ref 24), the eutectic structure is composed of β_1-Ni_3Si and α-Ni phases. When 10% TiC is added, the TiC phase is aggregation in the composite (shown in Fig. 2b). The structures of the matrix alloys are more homogeneous as the content of TiC increases (shown in Fig. 2c and d). This is because the higher sintering temperature and the aggregation of TiC promote the reaction among the elements. It should be noted that there are some micropores in the composite with high TiC addition compared to Ni_3Si alloy. But the micropores are mainly concentrated in the TiC phase, and this indicates that the high content of TiC makes the composite hard to be densified.

The relative densities of the composites with different TiC content are shown in Fig. 3. The sample without TiC addition exhibits the highest relative density, and the value is above 98%. In general, the high sintering temperature and high heat release are beneficial to the compaction and densification of the materials during the hot-pressing sintering process. The high relative density of this sample can attribute to the high sintering temperature and high reaction heat of Ni with Si and Ti. With the addition of TiC, Ni_3Si alloy content decreases in the composite, which leads to a decrease in the reaction heat. The lower content of the matrix alloy, the lower heat release. In order to achieve the high relative density of the sintered material, the sintering temperature must be higher. Therefore, the composites with higher content of TiC have higher sintering temperature. The two opposite effects on sintering process result in a maximum value of the relative densities of the composites, and so the relative density of the composite containing 20% TiC is a little higher than those of the composites containing 10 and 30% TiC.

The microhardnesses of the composites are shown in Fig. 4. The results show that the hardness of the composite with 10 wt.% TiC addition is close to that of Ni_3Si alloy. This is because the composite shows poor densification and a lower content of γ phase, whereas Ni_3Si alloy exhibits higher densification and high content of γ phase. The hardness of the composites with 20 wt.% TiC addition increases significantly with the further increase in TiC content, which is attributed to the high content of TiC and high relative density. It is worth noting that although the composite with 30% TiC addition presents some micropores (shown in Fig. 2d), it still has the highest hardness. The high sintering temperature makes the reaction of Ni with Si and Ti more completely, and the in situ matrix alloy is compacted during the hot-pressed process. However, there are some defects in the aggregation area of TiC phase that is hard to fully densify. Consequently,
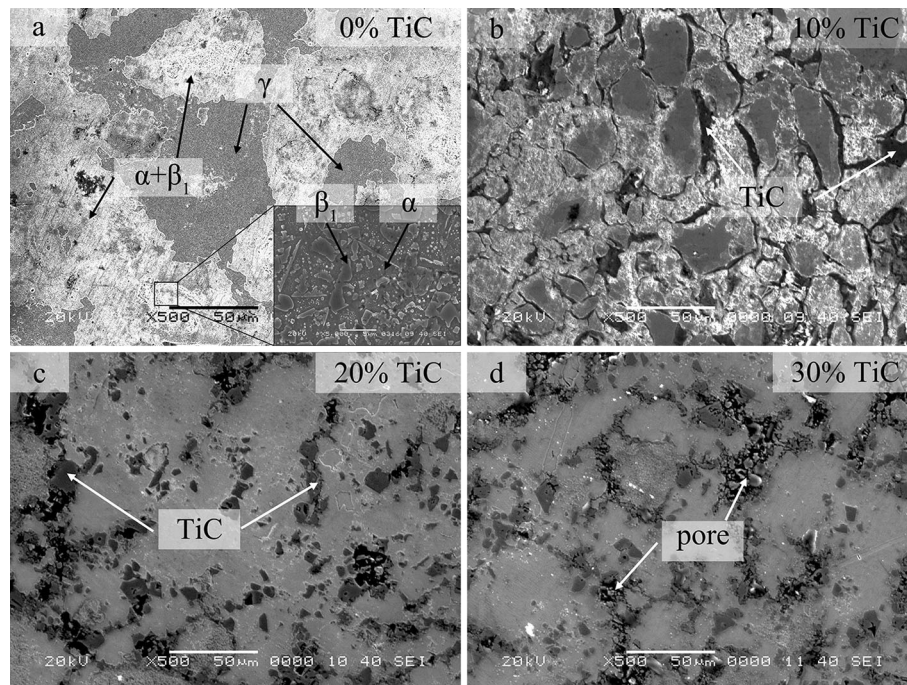

Fig. 2 SEM micrographs of Ni3Si-TiC composites: (a) 0 wt.% TiC, (b) 10 wt.% TiC, (c) 20 wt.% TiC, (d) 30 wt.% TiC
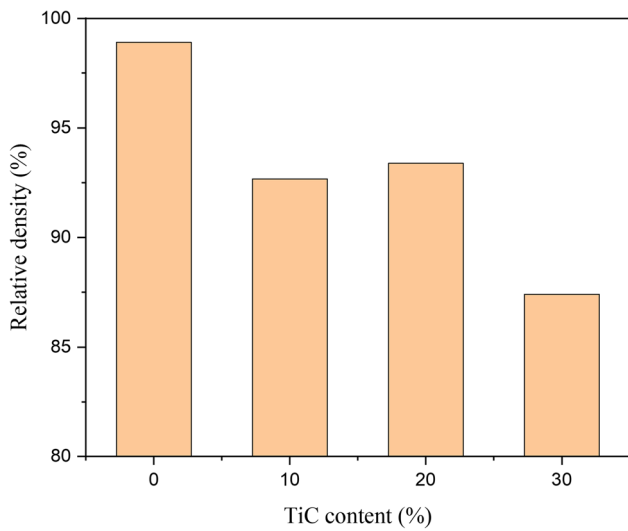
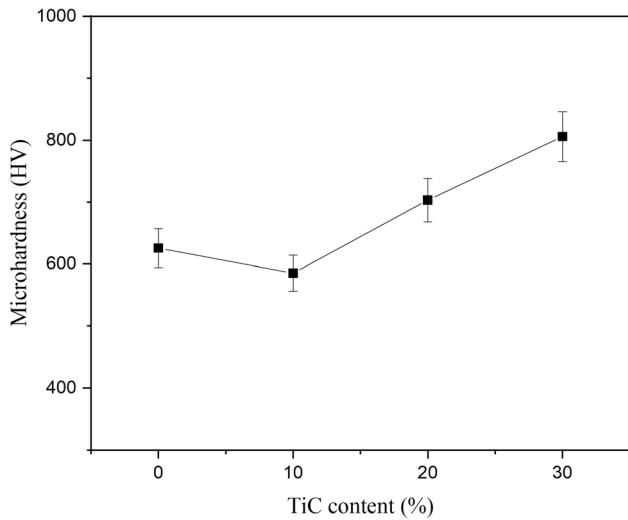**Fig. 3** Relative densities of Ni₃Si-TiC composites with different TiC content

Fig. 4 Effect of TiC content on the hardness of the composites

Fig. 5 Variations of the friction coefficients of the composites with the applied load
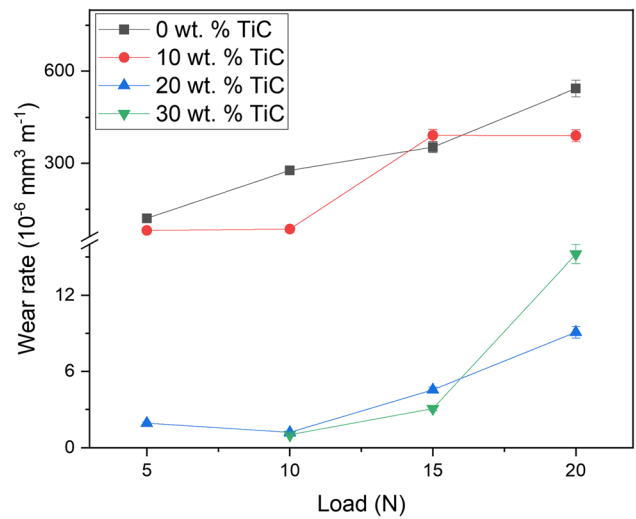
Fig. 6 Variations of the wear rates of the composites with the applied load

the compact matrix alloy provides good bearing capacity, and the composite has a higher hardness.

3.2 Tribological Properties of the Composites

Figure 5 shows the average friction coefficients of the composites with different TiC content. It is observed that the friction coefficients of the composites are all below 0.22, and the composites show good anti-friction performance. The previous study indicates that Ni_3Si materials exhibit high coefficients of friction (about 0.5) (Ref 14). It has also been reported that the oxidation resistance of Ni_3Si is reduced by the addition of Ti (Ref 25, 26). Accordingly, the low friction coefficient may be due to surface oxidation, and the oxide layer prevents direct contact with the surface asperities (Ref 27). The friction coefficient of Ni_3Si alloy decreases with increasing load. The high relative density of Ni_3Si alloy effectively prevents the oxidation of the inner layer during the friction process, but the oxidation gradually increases with the increase of load. Furthermore, the oxide layer reduces the friction
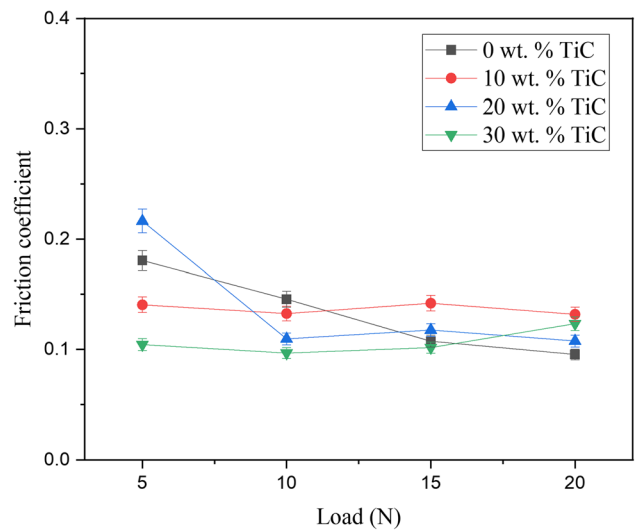
coefficient as the load increases. As compared to Ni_3Si alloy and the composite with 10% TiC, the composite with 20% TiC has a good relative density and low content of the Ni-Si phase, and thus, it presents a higher friction coefficient at the load of 5 N. At high loads, the defects cause severe oxidation, which generates the similar surface contact between the tribopairs. As a result, the friction coefficient of all the composite with TiC addition remains almost constant at high loads. In addition, the friction coefficient of the composites decreases with increasing TiC content at high loads, and this is because of the hardness.

The variations of wear rates of the composites with load at a sliding speed of 0.10 m/s are shown in Fig. 6. All the wear rates increase with increasing load. The wear resistance of the composite is higher than that of Ni_3Si alloy. The sample with 10% TiC has higher wear resistance and lower hardness compared to the alloy, whose wear rates are all in the order of 1×10^{-4} mm³ m⁻¹. The reason is that the high hardness of the TiC phase plays a role in the wear resistance. While the wear

rate of Ni_3Si alloy is the highest among the samples, it is still an order of magnitude lower than that in the previous study (Ref 19). Remarkably, the wear rates of the composites with 20% and 30% TiC are much lower, and all in the order of 1×10^{-6} $mm^3 \ m^{-1}$. It means that the high content of TiC significantly improves the wear resistance of the composites, which is two magnitudes higher than that of Ni_3Si alloy. The wear rates of the samples decrease roughly with increasing TiC content, and the composite with 20% TiC exhibits the optimal wear resistance.

Figure 7 shows the worn surfaces of the composites without and with 10% TiC at different loads. It can be seen that some fine debris particles and shallow furrows disperse on the worn surface of Ni_3Si alloy at the load of 10 N, as shown in Fig. 7 (a). The oxide particles are squeezed and then compacted to form an oxide layer on the worn surface when the applied load is 20 N (shown in Fig. 7b). The formation of the oxide layer causes the lowest friction coefficient to the alloy at the load. It should point out that the oxide layer is in the process of continuous spallation and reconstruction during the sliding friction. The wear mechanism of the alloy is mainly oxidation wear and slight abrasive wear. The morphologies of the worn surface of the composite with 10% TiC are markedly different from that of Ni_3Si alloy, as shown in Fig. 7 (c) and (d). A gray oxide layer already forms at low load, but the local area appears to peel off in flakes. The oxide layer, of which composition is 15.19Ni-14.15Si-2.03Ti-60.94O-7.69C, contains high content of silicon. The friction coefficients of the composite fluctuate slightly around 0.14 in the test range. The formation of the oxide layer and the exposure of the fresh surface of the composite cause the similar surface contact between the tribopairs and make the friction coefficients almost constant as the load increases. Moreover, there are some pits on the worn surface, and this indicates that the wear mechanisms of the composite are oxidation wear and fatigue wear under both loads.
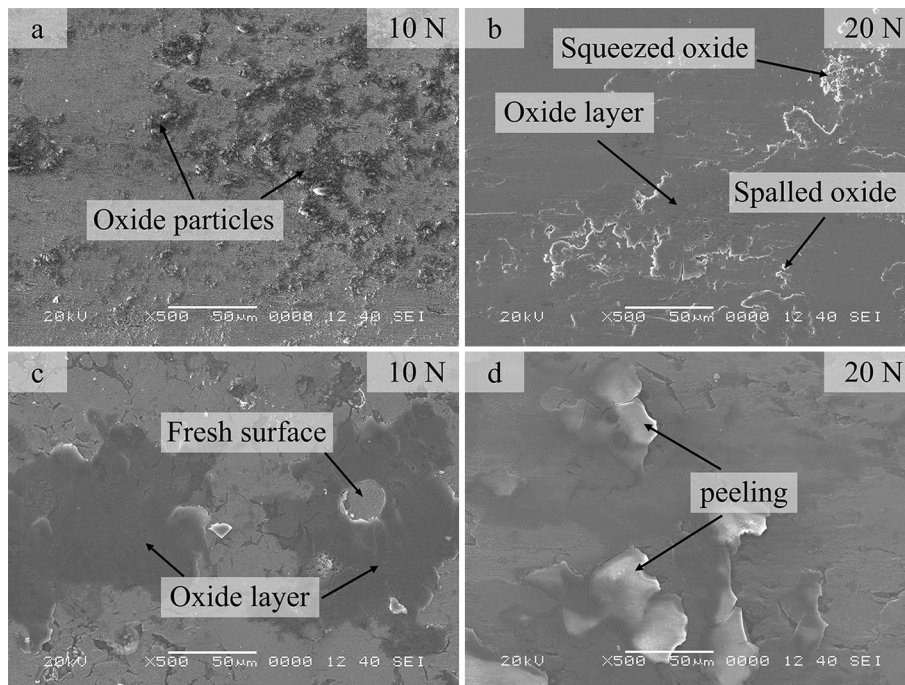
Figure 8 shows the SEM images of worn surfaces of the composites with 20% and 30% TiC at different loads. The morphologies of both composites are similar to that of the composite with 10% TiC. The oxide layers and some spalling pits are also observed on the worn surface of both samples. The wear mechanisms of both composites are oxidation wear and fatigue wear. Surprisingly, the oxide layers of the two composites have a higher silicon content compared to the composite with 10% TiC. The average compositions of both oxide layers are 8.80Ni-13.99Si-3.06Ti-66.73O-7.82C (20% TiC) and 5.63Ni-14.41Si-4.13Ti-68.35O-7.48C (30% TiC), respectively. However, the silicon contents of the two composites decrease with increasing TiC content, which are contradictory to the above results. A possible reason is that silicon transfers from the Si_3N_4 ball to the oxide layer.

Figure 9 shows the SEM images of worn surfaces of the counterpart ball sliding against different samples. For the Ni_3Si/Si_3N_4 tribopair, it can be seen that there are some shallow grooves and wear debris on the worn surface of Si_3N_4 ball (shown in Fig. 9a). The main wear mechanism is slightly abrasive wear. But when the counterpart ball slides against the composite with 20% TiC addition, the worn surface of the ball appears some spalling (shown in Fig. 9b). The main wear mechanism of the ball is fatigue wear. Consequently, the wear mechanisms of the counterpart balls are consistent with the results of the above analysis.

4. Discussion

Nickel-silicon is a low exothermic system, and the adiabatic temperature of Ni_3Si is 2250 K (Ref 16), which is higher than the melting temperature of the alloy. Some studies have shown that the reaction temperature can be as low as 790 °C (Ref 17). During the sintering process, Ni reacts with Si to form the Ni_2Si
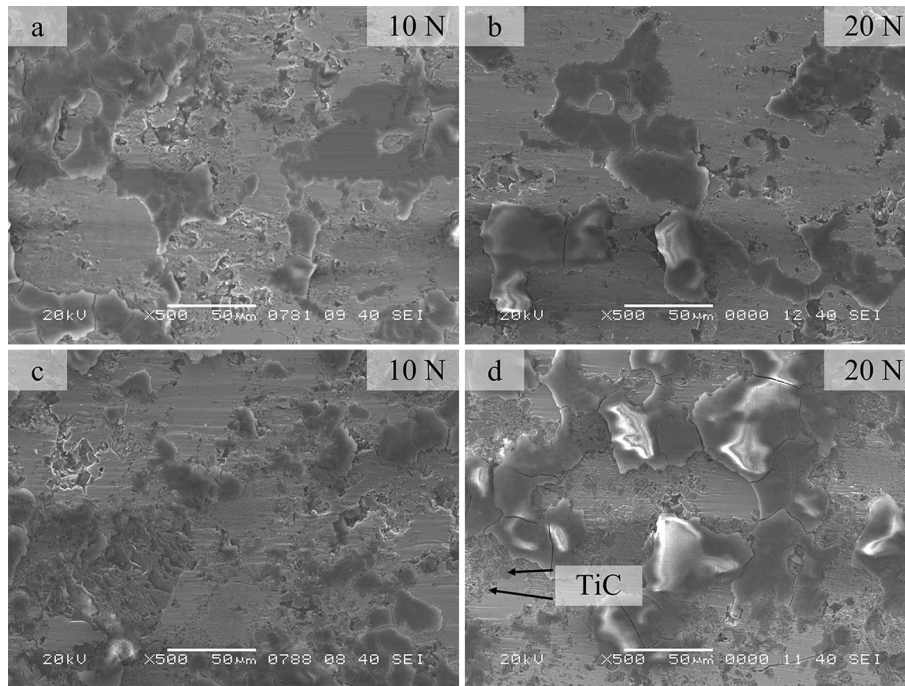

Fig. 7 SEM morphologies of worn surface at different loads: (a) and (b) 0% TiC; (c) and (d) 10% TiC

Fig. 8 SEM morphologies of worn surface at different loads: (a) and (b) 20% TiC; (c) and (d) 30% TiC
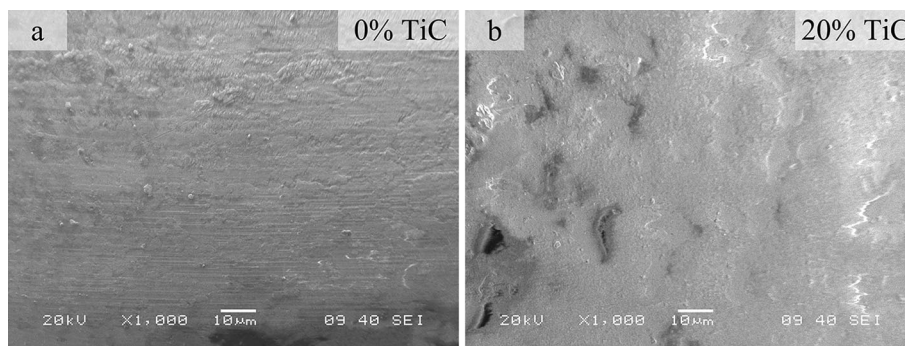

Fig. 9 SEM morphologies of worn surfaces of the counterpart balls sliding against different samples at 20 N: (a) 0% TiC, (b) 20% TiC

phase, and the high exothermic heat of the reaction causes local melting in the alloy (Ref 17). The fusion occurs easily in the liquid region, and the liquid Ni-Si phase further reacts with the surrounding Ni to form the γ phase. Meanwhile, the Ti particles migrate and aggregate gradually in the local area. With the formation of the γ phase, the liquid phase is consumed and disappears, so the region of the γ phase is almost free of titanium, as shown in Fig. 2(a). As the sintering temperature rises, the reactions in the Ti-rich region begin to take place near the eutectic points of Ni-Si-Ti (Ref 24). Finally, the eutectic structure of β_1 and α phases forms. The phase composition of Ni_3Si alloy with Ti addition is α-Ni, β_1-Ni_3Si, and a small amount of γ-$Ni_{31}Si_{12}$. With the addition TiC particles, the particles do not react with the elemental powders. The particles become gradually agglomeration as the reaction among the elements. The agglomeration of TiC particles separates the blended elemental powders into a small area and prevents the elemental particles from migration and aggregation over an extensive range. Then the Ni and Ti particles can still react with the γ phase and promote the transformation of the γ phase into

the β_1 phase during the sintering process (Ref 28). The main phase compositions of the composites with TiC addition are β_1-Ni_3Si and TiC phases. Therefore, there is almost no Ti-rich area in the matrix alloys, of which compositions are more homogeneous compared to Ni_3Si alloy. It is worth noting that the diffraction peaks of Ni_3Si phase shift to lower angles in all the samples, and this is due to the partial substitution of Si by Ti in Ni_3Si unit cell (Ref 29). The more the content of solid solution titanium is, the bigger the peak of Ni_3Si phase deviates.

From the above analysis, Ni_3Si-TiC composites are successfully prepared by in situ reaction sintering, and the compositions of the matrix alloys are more uniform than that of Ni_3Si alloy. Besides, the lower wear rates indicate the composites have good adhesion between the matrix and TiC phase. Although the spalling pits are observed (shown in Fig. 8), the spallation only occurs between TiC particles rather than between the matrix and TiC particles. Single TiC particle is firmly embedded in the matrix (shown in Fig. 8d), and this aggravates the wear of the Si_3N_4 ball. The wear debris of Si_3N_4

is compacted on the worn surface, and thus the silicon content in the oxide layer increases significantly.

To verify this hypothesis, an XPS analysis was performed on the worn surface. Figure 10 shows the XPS spectra of Ni 2p and Ti 2p on the worn surface. As can be seen from the figure, the chemical states of Ni are similar in the samples with different TiC addition, as shown in Fig. 10(a). The peaks appeared at 855.9 eV, and 873.5 eV are ascribed to the Ni 2p3/2 and Ni 2p1/2 peaks of oxidized nickel (Ref 30, 31). The distinct peak around 861-862 eV can be ascribed to the shake-up satellite peak of NiO (Ref 32). A weak peak located at 853.1 eV (curve-fitted value) is attributed to nickel silicide (Ref 33, 34). The peaks at 852.5 eV and 869.6 eV are assigned to metallic Ni (Ref 35, 36). There is a shake-up satellite peak of metallic Ni at about 858.4 eV (Ref 37, 38). The results indicate that nickel element exists in the forms of Ni (0) species and NiO species on both worn surfaces. However, the chemical states of Ti are different in the samples with different TiC addition, as shown in Fig. 10(b). For the sample without TiC addition, the peak at 454.1 eV is detected on the worn surface and assigned to metallic titanium (Ref 39). The fitting peak at 454.5 eV corresponds to the binding energies of TiNi (Ref 40, 41), and the peak located around 458.9 eV can be attributed to silicon-coated TiO_2 (Ref 42). For the sample with 20% TiC addition, the peaks at 454.4 eV and 460.4 eV are ascribed to the Ti 2p3/2 and Ti 2p1/2 peaks of TiC (Ref 43). The peak at 455.3 eV corresponds to TiO species (Ref 44), and this is probably due to the partial oxidation during the friction process. In addition, the peaks at 458.4 eV and 464.1 eV are attributed to Ti 2p3/2 and Ti 2p1/2 of TiO_2 in both samples (Ref 45, 46). From the above analysis, it is concluded that it is free of metallic Ti on the worn surface of the composites with 20% TiC. This means that Ti reacts with Ni-Si thoroughly and is not aggregation in the matrix. Therefore, the composition of the matrix alloy is more uniform than that of Ni_3Si alloy.

Figure 11 shows the XPS spectra of Si 2p on the worn surface. The peak at 99 eV is related to Si-Si bonds in both samples. The very low content of pure silicon in the composite with 20% TiC indicates that the Si element has a good reaction with the Ni element. Since the sample without TiC contains almost no nitrogen, the peaks at 101 eV, 101.8 eV, 102.4 eV, and 103.5 eV are all different chemical species of silicon oxides

on the worn surface (Ref 47-49), and they may be related to SiO_x, Si-O-Ti, Si-O-Si, and SiO_2, respectively. The peak at 103.1 eV also indicates the presence of SiO_2 in the sample with 20% TiC (Ref 50). The difference is that the sample with TiC addition contains nitrogen, and thus, the peaks at 101.6-102.3 eV are attributed to Si 2p of Si_3N_4 (Ref 51). It can conclude that the Si_3N_4 species on the worn surface comes from the Si_3N_4 balls. Although the hardness of Si_3N_4 is much higher than those of the composites, TiC possesses higher hardness than Si_3N_4. Parts of TiC particles are firmly embedded in the matrix alloy and cause the wear of the Si_3N_4 ball instead of TiC particles being pulled out. Therefore, the composites with the addition of TiC exhibit excellent wear resistance, and the wear rates of the composites are about two orders of magnitude lower than that of Ni_3Si alloy. Moreover, the debris forms an oxide layer that contains many brittle Si_3N_4 particles. The brittle oxide layer is easy to crack and peel off even at low loads.
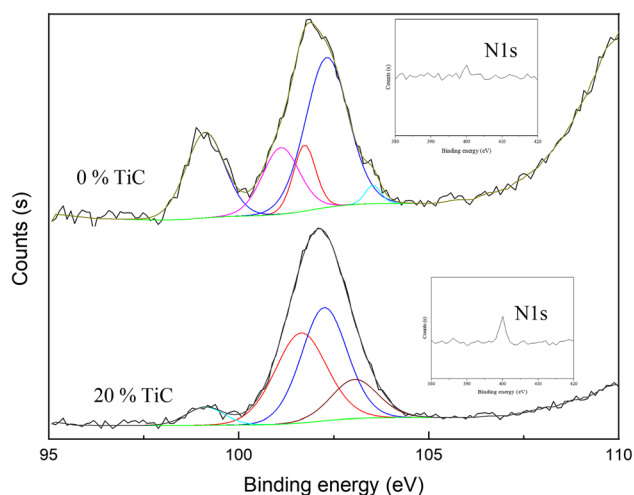

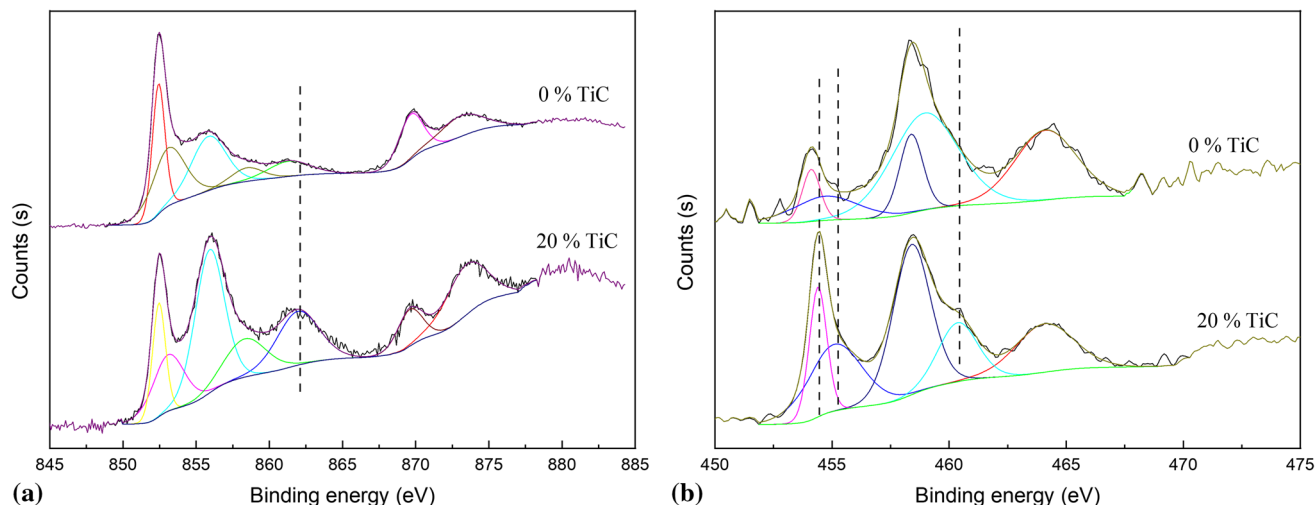**Fig. 11** XPS spectra of Si2p on the worn surfaces of the samples without and with 20% TiC addition at 20 N

Fig. 10 XPS spectra of Ni2p (a) and Ti2p (b) on the worn surfaces of the samples without and with 20% TiC addition at 20 N

5. Conclusions

Ni$_3$Si-TiC composites were fabricated by in situ reaction sintering. The phase composition, microstructure, and mechanical and tribological properties of the composites were investigated in this work. The main conclusions are summarized as follows:

(1) Ni$_3$Si-TiC composites are successfully fabricated by in situ reaction sintering method. The main phase composition of Ni$_3$Si alloy is α-Ni, β_1-Ni$_3$Si, and a small amount of γ-Ni$_{31}$Si$_{12}$, but the composites with the addition of TiC are β_1-Ni$_3$Si and TiC. The reason for this is that the TiC phase prevents the elemental particles from migration and aggregation over an extensive range, and the Ti and Ni particles can thoroughly react with the γ phase to form β_1 phase in the matrix alloy.

(2) The prepared composites have high hardness and relative density. The microhardnesses are all above 580 HV and almost increase with the increase of TiC content; the relative densities are still above 92% when the content of TiC is up to 20%. A small number of defects are mainly located in the aggregation area of TiC rather than at the interface between the matrix and TiC particles.

(3) The friction coefficients of the composites are below 0.22. At high loads, the friction coefficients of the composites with TiC addition are almost constant under different loads, and the value decreases with increasing TiC content. The composites exhibit excellent wear resistance. The wear rates of the composites with high content TiC are two orders of magnitude lower than that of Ni$_3$Si alloy. The composite with 20% TiC addition shows the optimal wear resistance in the test range, and the wear rate is in the order of 10^{-6} mm^3 m^{-1}.

(4) The Si content on the worn surface increases with the increasing TiC content in the composites. This is because the high hardness of TiC causes the wear of Si$_3$N$_4$ ball and significantly improves the tribological properties of Ni$_3$Si-based composites. The primary wear mechanism of Ni$_3$Si alloy is oxidation wear and slight abrasive wear, and the composites with TiC addition are oxidation wear and fatigue wear.

References

1. T. Takasugi, C.T. Liu, L. Heatherly, E.H. Lee and E.P. George, Boron Contaminations and their Kinetics in Ni$_3$(Si, Ti) Alloys, *Intermetallics*, 1998, **6**(5), p 369–377.
2. T. Takasugi and S. Hanada, The Influence of Second-Phase Dispersion on Environmental Embrittlement of Ni$_3$(Si, Ti) Alloys, *MRS Proceedings*, 1998, **552**, p 1–6.
3. C.M. Ward-Close, R. Minor ,and P.J. Doorbar, Intermetallic-Matrix Composites—A Review, *Intermetallics*, 1996, **4**(3), p 217–229.
4. S.Q. Wang, X.X. Li, K.M. Chen ,and H.J. Jin, TiC/Ni3Al Coating on Steel Via Combustion Synthesis During Casting, *Mater. Lett.*, 2007, **61**(11–12), p 2531–2534.
5. S.Y. Zhu, Q.L. Bi, J. Yang, W.M. Liu ,and Q.J. Xue, Ni$_3$Al Matrix High Temperature Self-Lubricating Composites, *Tribol. Int.*, 2011, **44**(4), p 445–453.
6. H. Liu, X. Zhang, Y. Jiang ,and R. Zhou, Microstructure and High Temperature Oxidation Resistance of in-Situ Synthesized TiN/Ti$_3$Al Intermetallic Composite Coatings on Ti6Al4V Alloy by Laser Cladding Process, *J. Alloys Compd.*, 2016, **670**, p 268–274.
7. M.Y. Niu, Q.L. Bi, J. Yang ,and W.M. Liu, Tribological Performances of Ni$_3$Si–Cr$_7$C$_3$ Composite Coatings Under Water and Acid Environments, *Tribol. Int.*, 2012, **48**, p 216–225.
8. T. Takasugi, H. Kawai ,and Y. Kaneno, The Effect of Cr Addition on Mechanical and Chemical Properties of Ni$_3$Si Alloys, *Mater. Sci. Eng. A*, 2002, **329–331**, p 446–454.
9. T. Takasugi, Microstructure and Tensile Properties of Ni$_3$ (Si, Ti) Alloys Containing Second Phase Dispersions, *Mater. Sci. Technol.*, 2000, **16**, p 73–80.
10. T. Takasugi, Microstructural Control and Mechanical Properties of Nickel Silicides, *Intermetallics*, 2000, **8**(5–6), p 575–584.
11. X.D. Lu, H.M. Wang and Z.R. Zhou, Reciprocating Sliding Wear Behavior of Laser-Clad Small Amplitude Mo$_2$Ni$_3$Si/NiSi Metal Silicide Composite Coatings, *Appl. Surf. Sci.*, 2005, **240**(1–4), p 432–440.
12. Y. Wang, and H.M. Wang, Wear Resistance of Laser Clad Ti$_2$Ni$_3$Si Reinforced Intermetallic Composite Coatings on Titanium Alloy, *Appl. Surf. Sci.*, 2004, **229**(1–4), p 81–86.
13. X.D. Lu and H.M. Wang, High-Temperature Phase Stability and Tribological Properties of Laser Clad Mo$_2$Ni$_3$Si/NiSi Metal Silicide Coatings, *Acta Mater.*, 2004, **52**(18), p 5419–5426.
14. M.Y. Niu, Q.L. Bi, L.Q. Kong, J. Yang ,and W.M. Liu, A Study of Ni$_3$Si-Based Composite Coating Fabricated by Self-Propagating High Temperature Synthesis Casting Route, *Surf. Coat. Technol.*, 2011, **205**(17–18), p 4249–4253.
15. Y.Q. Pu, Q.L. Bi, J. Yang, J.M. Chen ,and Q.J. Xue, Effects of C Alloying on Microstructure and Properties of Ni-Si-Cr Ternary Alloys, *Mater. Sci. Eng. A*, 2008, **496**(1–2), p 316–322.
16. Q.L. Bi, P.Q. La, W.M. Liu, Q.J. Xue ,and Y.T. Ding, Microstructure and Properties of Ni$_3$Si Alloyed with Cr Fabricated by Self-Propagating High-Temperature Synthesis Casting Route, *Metall. Mater. Trans. A*, 2005, **36**, p 1301–1307.
17. S. Van Dyck, L. Delaey, L. Froyen ,and L. Buekenhout, Reactive Powder Metallurgy of Ni$_3$Si-Based Alloys, *Intermetallics*, 1995, **3**(4), p 309–314.
18. Y. Miura, Y. Kaneno, T. Takasugi ,and A. Kakituji, Characterization of Ni$_3$(Si, Ti) Intermetalic Alloys Synthesized by Powder Metallurgical Method, *MRS Proc.*, 2013, **1516**, p 121–126.
19. X. Zhang, M. Niu, C. Wu ,and J. Chen, The Effect of Titanium Addition on the Microstructure, Mechanical and Tribological Properties of Ni$_3$Si Alloys Prepared by Powder Metallurgy Method, *Materialwiss. Werkst.*, 2019, **50**(12), p 1537–1544.
20. C. Wu, M. Niu, S. Bao, Y. Sun ,and X. Zhang, Friction and Wear Properties of Ni$_3$Si Alloy with Ti Addition at High Temperatures, *Materials*, 2020, **13**(4), p 982.
21. M. Niu, X. Zhang, J. Chen ,and X. Yang, Friction and Wear Properties of Ni$_3$Si Alloy Under Different Vacuum Conditions, *Vacuum*, 2019, **161**, p 443–449.
22. M. Niu, X. Zhang, F. Tu ,and J. Liang, The Tribological Properties of Ni$_3$Si Alloys with Ti Addition Against Different Counterface Materials Under Seawater Condition, *Mater. Res. Express*, 2018, **5**(11), 116533.
23. T. Takasugi, O. Izumi ,and M. Yoshida, Mechanical Properties of Recrystallized L1$_2$-type Ni$_3$(Si, Ti) Intermetallics, *J. Mater. Sci.*, 1991, **26**(5), p 1173–1178.
24. F. Weitzer, M. Naka, N. Krendelsberger, F. Stein, C. He, Y. Du ,and J.C. Schuster, The Ternary System Nickel/Silicon/Titanium Revisited Zeitschrift für anorganische und allgemeine, *Chemie*, 2010, **636**(6), p 982–990.
25. Y. Fujimoto, Y. Kaneno ,and T. Takasugi, Alloying Effect on Mechanical Properties and Oxidation Resistance of Cold-Rolled Ni$_3$(Si, Ti) foils, *Mater. Res. Soc. Symp. Proc.*, 2009, **1128**, p 245–250.

26. T. Takasugi, H. Kawai ,and Y. Kaneno, Mechanical and Chemical Properties of Ni$_3$Si and Ni$_3$(Si, Ti) Alloys Multiphased by Chromium Addition, *Mater. Sci. Technol.*, 2001, **17**, p 671–680.

27. K.C. Ludema, O.O. Ajayi, Friction, Wear, Lubrication: A Textbook in Tribology (2nd ed.), 2nd ed., CRC Press, 2018

28. T. Takasugi, D. Shindo, O. Izumi ,and M. Hirabayashi, Metallographic and Structural Observations in the Pseudo-Binary Section Ni$_3$Si-Ni$_3$Ti of the Ni-Si-Ti System, *Acta Metall. Mater.*, 1990, **38**(5), p 739–745.

29. T. Takasugi, M. Nagashima ,and O. Izumi, Strengthening and Ductilization of Ni$_3$Si by the Addition of Ti Elements, *Acta Metall. Mater.*, 1990, **38**(5), p 747–755.

30. G. Carja, E. Husanu, C. Gherasim ,and H. Iovu, Layered Double Hydroxides Reconstructed in NiSO$_4$ Aqueous Solution as Highly Efficient Photocatalysts for Degrading Two Industrial Dyes, *Appl. Catal. B*, 2011, **107**(3), p 253–259.

31. Z. Yu, D. Chen, M. Rønning, T. Vrålstad, E. Ochoa-Fernández, A. Holmen, Large-scale synthesis of carbon nanofibers on Ni-Fe-Al hydrotalcite derived catalysts: I. Preparation and characterization of the Ni–Fe–Al hydrotalcites and their derived catalysts, Appl. Catal. A: Gen., **338**(1), 136–146 (2008)

32. J. Li, F. Meng, S. Suri, W. Ding, F. Huang ,and N. Wu, Photoelectrochemical Performance Enhanced by a Nickel Oxide−Hematite p−n junction Photoanode, *Chem. Commun.*, 2012, **48**(66), p 8213–8215.

33. C. Hallin, R. Yakimova, B. Pécz, A. Georgieva, T. Marinova, L. Kasamakova, R. Kakanakov ,and E. Janzén, Improved Ni Ohmic Contact on n-type 4H-SiC, *J. Electron. Mater.*, 1997, **26**(3), p 119–122.

34. T. Marinova, V. Krastev, C. Hallin, R. Yakimova ,and E. Janzén, Interface Chemistry and Electric Characterisation of Nickel Metallisation on 6H-SiC, *Appl. Surf. Sci.*, 1996, **99**(2), p 119–125.

35. Y. Xu, J. Yang, T. Liao, R. Ge, Y. Liu, J. Zhang, Y. Li, M. Zhu, S. Li and W. Li, Bifunctional Water Splitting Enhancement by Manipulating Mo-H bonding Energy of Transition Metal-Mo$_2$C Heterostructure catalysts, *Chem. Eng. J.*, 2022, **431**, 134126.

36. X. Zhao and G. Lu, Improving Catalytic Activity and Stability by in-Situ Regeneration of Ni-Based Catalyst for Hydrogen Production from Ethanol Steam Reforming Via Controlling of Active Species Dispersion, *Int. J. Hydrogen Energy*, 2016, **41**(32), p 13993–14002.

37. J. Li, B.B. Yang, Y.H. Lu, L. Xin, Z.H. Wang ,and T. Shoji, The degradation Mechanism of Inconel 690TT Induced by Fretting Wear in Air, *Tribol. Int.*, 2017, **116**, p 147–154.

38. A. Busiakiewicz, W. Kozłowski, P. Dąbrowski, M. Rogala ,and Z. Klusek, Temperature-Induced Segregation of Co- and Ni-rich Nanoparticles on Rutile TiO$_2$(001), *Mater. Res. Express*, 2016, **3**(8), 085004.

39. X. Gai, Y. Bai, J. Li, S. Li, W. Hou, Y. Hao, X. Zhang, R. Yang ,and R.D.K. Misra, Electrochemical Behaviour of Passive Film Formed on the Surface of Ti-6Al-4V Alloys Fabricated by Electron Beam melting, *Corros. Sci.*, 2018, **145**, p 80–89.

40. C.L. Chu, R.M. Wang, T. Hu, L.H. Yin, Y.P. Pu, P.H. Lin, S.L. Wu, C.Y. Chung, K.W.K. Yeung ,and P.K. Chu, Surface Structure and Biomedical Properties of Chemically Polished and Electropolished NiTi Shape Memory Alloys, *Mater. Sci. Eng., C*, 2008, **28**(8), p 1430–1434.

41. C.L. Chu, C.Y. Chung, J. Zhou, Y.P. Pu ,and P.H. Lin, Fabrication and Characteristics of Bioactive Sodium Titanate/Titania Graded Film on NiTi Shape Memory Alloy, *J Biomed Mater Res A*, 2005, **75A**(3), p 595–602.

42. Y.-L. Lin, T.-J. Wang ,and Y. Jin, Surface Characteristics of Hydrous Silica-Coated TiO$_2$ Particles, *Powder Technol.*, 2002, **123**(2), p 194–198.

43. Y. Qin and M. Hu, Characterization and Field Emission Characteristics of Carbon Nanotubes Modified by Titanium Carbide, *Appl. Surf. Sci.*, 2008, **254**(11), p 3313–3317.

44. S. Kim and S.K. Lim, Preparation of TiO$_2$-Embedded Carbon Nanofibers and their Photocatalytic Activity in the Oxidation of Gaseous Acetaldehyde, *Appl. Catal. B*, 2008, **84**(1), p 16–20.

45. J. Du, J. Zhang, Z. Liu, B. Han, T. Jiang ,and Y. Huang, Controlled Synthesis of Ag/TiO$_2$ Core−Shell Nanowires with Smooth and Bristled Surfaces via a One-Step Solution Route, *Langmuir*, 2006, **22**(3), p 1307–1312.

46. Q. Ling, J. Sun ,and Q. Zhou, Preparation and Characterization of Visible-Light-Driven Titania Photocatalyst Co-Doped with Boron and Nitrogen, *Appl. Surf. Sci.*, 2008, **254**(10), p 3236–3241.

47. W.A.M. Aarnink, A. Weishaupt ,and A. van Silfhout, Angle-Resolved X-Ray Photoelectron Spectroscopy (ARXPS) and a Modified Levenberg-Marquardt Fit Procedure: a New Combination for Modeling Thin Layers, *Appl. Surf. Sci.*, 1990, **45**(1), p 37–48.

48. B. Deng, J. Li, H. Shang, W. Liu, Q. Wan, M. Chen, M. Qu, G. Peng (2020) Improving cyclic stability of LiNi$_{0.6}$Co$_{0.2}$Mn$_{0.2}$O$_2$-SiO$_x$/graphite full cell using tris(trimethylsilyl)phosphite and fluoroethylene carbonate as combinative electrolyte additive, *Ionics*, **26**(5), 2247–2257

49. K.J. Kim, D.W. Moon, S.H. Nam, W.J. Lee and H.G. Kim, XPS Sputter Depth Profiling of the Chemical States for SrTiO$_3$/Si Interface by O$_2^+$ Ion Beams, *Surf. Interface Anal.*, 1995, **23**(13), p 851–857.

50. M. Garza, J. Liu, N.P. Magtoto and J.A. Kelber, Adhesion Behavior of Electroless Deposited Cu on Pt/Ta Silicate and Pt/SiO$_2$, *Appl. Surf. Sci.*, 2004, **222**(1), p 253–262.

51. P. Zhang, Z. Cai and W. Xiong, Influence of Si Content and Growth Condition on the Microstructure and Mechanical Properties of Ti-Si-N Nanocomposite Films, *Surf. Coat. Technol.*, 2007, **201**(15), p 6819–6823.